AGU ADVANCING EARTH AND SPACE SCIENCES

Geophysical Research Letters

RESEARCH LETTER
10.1029/2025GL120545

The Influence of Tropopause Temperature Biases on Climate Model Simulations of Tropical Cyclones

Aidan D. Mahoney[1], Brian J. Soden[1], Bosong Zhang[2], and Gabriel Vecchi[3,4]

[1]Rosenstiel School of Marine, Atmospheric, and Earth Science, University of Miami, Miami, FL, USA, [2]Program in Atmospheric and Oceanic Sciences, Princeton University, Princeton, NJ, USA, [3]Department of Geosciences, Princeton University, Princeton, NJ, USA, [4]High Meadows Environmental Institute, Princeton University, Princeton, NJ, USA

Key Points:

- Climate models exhibit large inter-model differences in temperature at and above the tropopause level
- The resulting inter-model spread in outflow temperature produces substantially different tropical cyclone potential intensities
- These differences in potential intensity induce biases in climate model simulations of global tropical cyclone intensity and frequency

Supporting Information:

Supporting Information may be found in the online version of this article.

Correspondence to:

A. D. Mahoney,
aidan.mahoney@miami.edu

Citation:

Mahoney, A. D., Soden, B. J., Zhang, B., & Vecchi, G. (2026). The Influence of tropopause temperature biases on climate model simulations of tropical cyclones. *Geophysical Research Letters*, *53*, e2025GL120545. https://doi.org/10.1029/2025GL120545

Received 7 NOV 2025
Accepted 7 FEB 2026

Abstract Potential intensity (PI) is a key indicator for tropical cyclone (TC) activity, yet it exhibits considerable variability across global climate model (GCM) simulations, even with identical sea surface temperatures (SSTs). We show that the spread in PI across GCMs is primarily driven by differences in outflow temperature, a consequence of different upper atmospheric temperatures. To explore the impacts of these biases on TC activity, we conduct several idealized experiments with altered temperature profiles. In these experiments, global TC frequency and accumulated cyclone energy change by ∼35% and hurricane frequency by ∼80%. There are smaller but still significant impacts on lifetime maximum intensity. These findings highlight an underappreciated role of upper atmospheric model biases in modulating TC activity in GCMs, how future changes in TC activity may be influenced by responses of upper atmospheric temperature to anthropogenic emissions, and that TCs are more directly influenced by PI than SST alone.

Plain Language Summary The maximum potential intensity (PI) of tropical cyclones (TCs) differs across GCMs, despite these GCMs using identical SSTs. We show that these differences in PI are driven by different temperature conditions in the upper atmosphere, specifically at the tropopause and within the lower stratosphere. Cooler tropopause temperatures produce cooler outflow temperatures, which results in a higher PI and vice-versa. Differences in PI can affect long-term average TC activity within these GCMs, especially TC intensity. Using a single high-resolution GCM capable of producing realistic global TCs we modify the upper atmospheric temperatures to investigate their impacts on TC activity. We find a significant relationship between upper atmospheric temperatures, PI, and resolved TC activity. The simulations with cooler upper atmospheric temperatures and higher PI produce stronger and more frequent TCs. This suggests that upper atmospheric temperatures can influence future changes in TC activity due to climate change, in addition to the already well-documented dependence on surface temperature.

1. Introduction

Tropical cyclones (TCs) pose multiple threats to human life and property (Klotzbach et al., 2018; Rappaport, 2014). In a warming climate, TC intensity is projected to increase along with an increasing proportion of Category 4 and stronger TCs (Elsner et al., 2008; Knutson et al., 2020; Kossin et al., 2013, 2020). TC potential intensity (PI) represents the maximum possible intensity a TC could attain within a given thermodynamic environment (Bister & Emanuel, 1998; K. A. Emanuel, 1986) and is widely used to evaluate the large scale environment for tropical cyclogenesis and intensification (Bruyère et al., 2012; Camargo, Emanuel, & Sobel, 2007; Camargo et al., 2014; Camargo, Sobel, et al., 2007; Camargo & Wing, 2016; Chavas et al., 2024; Craig & Gray, 1996; K. Emanuel, 2010; K. A. Emanuel & Nolan, 2004; K. A. Emanuel et al., 1994; Sobel et al., 2016; Wang & Murakami, 2020). PI generally increases with anthropogenic warming and is widely believed to be the dominant driver behind climate model projections of increasing TC intensity (Bhatia et al., 2022; Knutson et al., 2020; Sobel et al., 2016; Walsh et al., 2016). The calculation of PI only considers the thermodynamic environment, for example, sea surface temperature (SST), mean sea level pressure, and vertical profiles of temperature and moisture. Unfavorable dynamics that inhibit TC formation and intensification, such as ventilation and vertical wind shear, are not considered in the computation of PI (Alland et al., 2021a, 2021b; Finocchio et al., 2016; Finocchio & Rios-Berrios, 2021; Rios-Berrios et al., 2024; Tang & Emanuel, 2010, 2012).

The theory of PI is derived from the efficiency of an idealized Carnot heat engine, where the warm ocean surface acts as the heat source and the outflow level, where the rising air parcels are expelled, acts as the heat sink. A

larger difference in temperature between the surface-level inflow and tropopause-level outflow allows for a more efficient heat engine and thus a larger PI (Bister & Emanuel, 1998; K. A. Emanuel, 1986). Thus, for a given value of SST, colder tropopause temperatures provide for colder outflow temperatures which contribute to larger values of PI (K. Emanuel et al., 2013; Kossin, 2015; Trabing et al., 2019; Vecchi et al., 2013; Wing et al., 2015). This is consistent with downscaling studies which find that cooler tropopause temperatures result in stronger TC intensities (K. Emanuel et al., 2013), and an increase in the proportion of hurricanes within global climate models (GCMs; Vecchi et al., 2013). We highlight that K. Emanuel et al. (2013), Vecchi et al. (2013) and Kossin (2015) all independently identified upper tropospheric temperature biases within reanalysis data that affect calculations of PI.

Broccoli and Manabe (1990) was one of the first studies to demonstrate the potential utility of GCMs for examining the impact of climate change on global TC activity; the study also identified that higher horizontal resolution would allow for the production of more realistic TC structures and intensities. Modern GCMs, like the models of the Coupled Model Intercomparison Project 6 (CMIP6), still insufficiently resolve TCs (Camargo et al., 2025). The High Resolution Model Intercomparison Project (HighResMIP) was designed to use the same forcings as CMIP6 but with finer horizontal resolutions of 25–50 km (Eyring et al., 2016; Haarsma et al., 2016). The HighResMIP GCMs have both atmosphere-only and coupled ocean-atmosphere configurations (Eyring et al., 2016; Haarsma et al., 2016). HighResMIP simulations have been shown to resolve TCs better than other GCMs with lower resolutions (Roberts et al., 2020a). Among the HighResMIP simulations, higher resolution models favor more frequent and stronger TCs with improved depictions of storm structure than lower resolution counterparts (Roberts et al., 2020a).

Despite these improvements in explicitly modeling TCs within GCMs, the observed TC climatology is not well reproduced in many models, and both historical and future trends in TC activity differ substantially between models (Kreussler et al., 2021; Roberts et al., 2020a, 2020b). For example, Roberts et al. (2020a) documented the difficulty of MPI-ESM1-2-XR to simulate any TCs, while the HadGEM-GC3.1-HM and CNRM-CM6-1-HR models were found to have anomalously high TC frequencies. Figure S1 in Supporting Information S1, which shows the locations of maximum TC intensity for HighResMIP models with TCs tracked using Tempest-Extremes, illustrates the large variance in TC frequency among the models. Moreover, while the highest resolution versions of each model were generally closest to observed intensity distributions, the models still largely fail to simulate TCs of category 4 and 5 strength (Roberts et al., 2020a). Some metrics of TC activity, like integrated kinetic energy, have been shown to be consistent across resolutions, but this is a consequence of significant differences in modeled TC structure (Kreussler et al., 2021).

Figure S2 compares tropical mean PI to mean TC lifetime maximum intensity (LMI), mean annual accumulated cyclone energy (ACE), and mean annual TC frequency. ACE is computed by integrating TC wind speed and duration (Bell et al., 2000). There are substantial intermodel differences in global TC activity, as measured by mean annual TC frequency, mean annual TC ACE, and mean TC LMI. These differences are not explained by the spread in PI, which agrees with Camargo et al. (2020) in that the large-scale environment does not fully explain intermodel differences in the TC climatology. Strong TCs (LMI >32 ms^{-1}) are poorly resolved in the ECMWF-IFS-HR, EC-Earth3P-HR, and MPI-ESM1-2-XR models (Roberts et al., 2020a) and these three models also produce the lowest average annual TC frequencies and annual TC ACE. These results suggest that while the HighResMIP models simulate substantial differences in their climatological PI, the spread in TC activity between these models is further complicated by the deficiencies in physical processes related to TC development (Camargo et al., 2020; Dirkes et al., 2023; Kim et al., 2018; Moon et al., 2020, 2022; Starr et al., 2025; Wing et al., 2019).

In this paper, we seek to better understand the cause of these large inter-model differences in TC activity and the potential role of tropopause and lower stratospheric temperature biases in contributing to these differences. Our focus will center on how these temperature biases affect the outflow temperature, PI, and TC activity. Section 2 describes computational and analysis methods, including the model simulations designed to test the influence of the upper atmospheric temperature profile on PI and TC activity. Section 3 reports results for PI and TC activity, and Section 4 provides a summary and conclusions.

2. Methods

For this work, we focus on the HighResMIP historical atmosphere-only simulations (highresSST-present) which use daily 0.25° HadISST2-based SST data as the oceanic surface boundary condition (Haarsma et al., 2016;

Kennedy et al., 2017). The period studied ranges from 1980 through 2014. This family of simulations is selected because the use of identical surface boundary conditions minimizes any differences in PI which would arise due to differences in SST. We note that other low-level conditions, for instance surface air temperature and humidity, differ insignificantly across these simulations. The highest resolution simulation of each model is selected since Roberts et al. (2020a) showed these best resolved TCs compared to lower resolution counterparts. Table S1 in Supporting Information S1 lists the models used in this study. The TRACK (Hodges et al., 2017) and TempestExtremes (Ullrich & Zarzycki, 2017; Zarzycki & Ullrich, 2017) TC tracking algorithms have been applied in prior work to the HighResMIP simulations during postprocessing of the model output (Roberts et al., 2020a). Reanalysis data from the ERA5 (Hersbach et al., 2020, 2023a, 2023b) and MERRA2 (Global Modeling And Assimilation Office & Pawson, 2015a, 2015b) data sets from 1980 to 2020 and 47 of the standard resolution CMIP6 AMIP models from 1980 to 2014 provide additional context for interpreting the climatological values of PI and tropopause temperatures.

PI is computed using the tcpyPI algorithm (Gilford, 2020, 2021), which follows the formulation derived in Bister and Emanuel (2002). The four inputs to the PI computation are SST, sea level pressure, and vertical profiles of temperature and specific humidity. All input variables are monthly averaged, and the PI is computed on each model's native grid resolution. Land areas are masked and individual ocean basins are defined using the RECCAP2-ocean regions toolkit from Gregor and Müller (2022). Throughout this paper, we adopt the broadly accepted boundaries of the regional TC basins: North Atlantic (NATL), Eastern North Pacific (EPAC), Central Pacific (CPAC), Western North Pacific (WPAC), North Indian Ocean (NIO), South Indian Ocean (SIO), South Pacific (SPAC), and South Atlantic (SATL). These basins are divided with reference to the equator, and include waters at all latitudes. In the North Pacific Ocean, the EPAC is bounded east of 140°W, the CPAC between 140°W and 180°, and the WPAC west of 180°.

For the calculation of PI, the ratio of the surface exchange coefficients is set to the default value of 0.9, dissipative heating is allowed, and air parcels are assumed to undergo pseudoadiabatic ascent. The minimum pressure level allowed is set to the default value of 50 hPa, at which level the PI calculation terminates and TC outflow level is assumed to be 50 hPa even if a parcel is still convectively unstable. The algorithm returns PI as scaled gradient wind speeds using the default reduction factor of 0.8, minimum central pressure, outflow temperature, and outflow temperature pressure level.

To counter the previously discussed limitations of HighResMIP and isolate the sensitivity of TC activity to differences in outflow temperature, we conduct a series of experiments using the National Oceanic and Atmospheric Administration's Geophysical Fluid Dynamics Laboratory High Resolution Atmospheric Model (HiRAM; Zhao et al., 2009), which has been shown to successfully simulate most of the observed TC climatology both globally and within individual TC basins (Camargo et al., 2014; Zhao et al., 2009, 2010; Zhao & Held, 2010, 2012). The model has a spatial resolution of ∼0.5°/50 km with 32 vertical model levels. HiRAM is forced by climatological monthly averaged SST and sea ice observed during the 1990s from HadISST (Rayner et al., 2003). To test the sensitivity of PI and TC activity to tropopause temperatures, model levels at and above the local tropopause are perturbed by ±4 K and ±8 K relative to the 12 monthly climatological temperature profiles in the control simulation. The nudging timescale is set to 1,200 s (20 min), and applied globally at every horizontal grid point. These temperature perturbations approximate the range in tropopause temperatures found in the HighResMIP models. The local tropopause is defined as the lowest level at which the lapse rate decreases to 2°C/km (World Meteorological Organization, 1957), using the same method as Mischell et al. (2024). This produces five HiRAM simulations for evaluation, four with perturbed tropopause and stratospheric temperatures and the unaltered control. Tropical mean (30°S–30°N) temperature profiles over open oceans from the HiRAM simulations is shown in Figure S3 in Supporting Information S1. TCs in the HiRAM simulations are tracked using the algorithm developed by Harris et al. (2016).

3. Results

3.1. Potential Intensity

Although all models in the HighResMIP simulations use identical SSTs, their simulated tropical mean (30°S to 30°N) PI values vary by ∼20%, ranging from ∼65 to 80 ms^{-1} (Figure 1a). Figure 1a compares the tropical mean PI from each HighResMIP model to the corresponding tropical mean outflow temperature. Also shown are the corresponding tropical mean PI and outflow temperature from 47 CMIP6 AMIP model simulations also using the

10.1029/2025GL120545

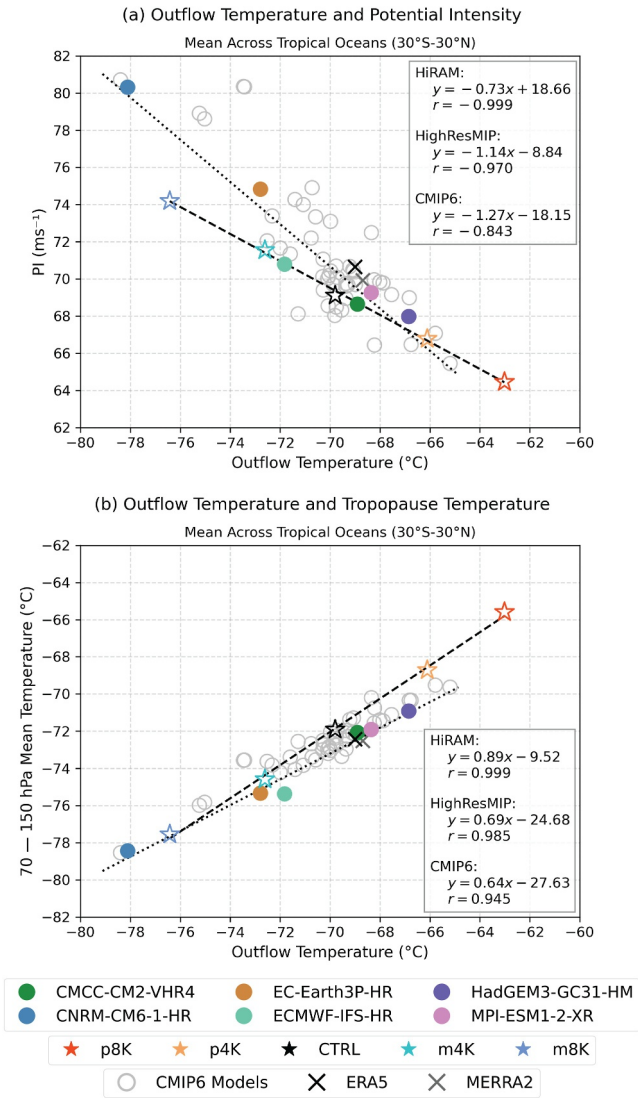

Figure 1. Tropical mean (a) potential intensity (PI) and (b) 70–150 hPa layer mean temperature compared to the outflow temperature over the open oceans. HighResMIP simulations are solid-colored circles. HiRAM simulations are indicated by stars. The 47 Coupled Model Intercomparison Project 6 models are gray open circles. Reanalysis data are marked with an X. Linear regression lines are plotted for HiRAM (dashed) and HighResMIP (dotted).

identical set of SSTs. Observational estimates of the tropical-mean outflow temperature from reanalyses are −69°C, whereas both CMIP6 and HighResMIP simulations range from roughly −65 to −78°C. This spread in outflow temperature is highly correlated to the inter-model differences in PI; models with colder outflow temperatures have larger values of PI and vice-versa. Figure 1a also includes the four HiRAM sensitivity experiments and the HiRAM control. While the HiRAM simulations also show a decrease in PI with increasing outflow temperatures, the sensitivity (0.7 ms^{-1} per 1°C of cooling) is noticeably smaller than that of the CMIP6/HighResMIP simulations (1.2 ms^{-1} per 1°C of cooling). Figure 1b relates outflow temperature to the tropopause temperature, which we take as the 70–150 hPa layer mean temperature. The tropopause temperature in HiRAM increases by 0.89°C per 1°C increase in outflow temperature, while HighResMIP and CMIP6 change by 0.69°C and 0.64°C, respectively. While outflow and tropopause temperature do not scale 1:1, they are closely related and indicate a significant response of the outflow temperature to the underlying tropopause temperature biases found in the models.

To better understand this difference in sensitivity of PI to outflow and tropopause temperature, we sort the CMIP6 and HighResMIP tropical ocean mean temperature profiles by their tropopause temperature into the coldest 25% and warmest 25% of the joint CMIP6/HighResMIP distribution (Figure 2). We then plot the difference of temperature profiles from the MERRA2 and ERA5 reanalysis mean. All CMIP6 models are cooler than reanalysis through most of the troposphere. Comparing just CMIP6, models with coolest tropopause temperatures are also cooler than their warmer counterparts in the troposphere. In contrast, the HiRAM simulations, by design, exhibit little difference in the temperature profile below the tropopause. This tropospheric cool bias increases PI by further depressing the outflow temperature. Thus, the larger sensitivity of PI to outflow temperatures in the HighResMIP and CMIP6 models reflects the influence of these co-varying biases. Because the HiRAM simulations do not include this covariance, the changes in PI are driven only by the change in outflow temperature due to differences in the upper atmospheric temperature profile. The sensitivity of PI to outflow temperatures found in the HiRAM, HighResMIP, and CMIP6 simulations is consistent with results described in Ramsay (2013), though that work used a regional model instead of our global model approach.

3.2. Tropical Cyclone Activity

Figure 3 compares the tropical mean PI to global average annual tropical cyclone frequency, global average annual ACE, and global mean TC LMI for each of the HiRAM sensitivity experiments. In this analysis, we only consider TCs with wind speeds of 17.5 ms^{-1} or stronger (tropical storms or stronger on the Saffir-Simpson Hurricane Wind Scale). The frequency of TCs is higher in cooler tropopause simulations (Figure 3). Average annual TC frequency ranges from 92 to 123, with the coolest tropopause simulation producing the most TCs. The average annual frequency of strong TCs (>32 ms^{-1}; Category 1 hurricanes and stronger) ranges from about 27 to 46, a near 70% increase from the warmest to coolest tropopause simulation at a rate of 2.5 strong TCs per 1 ms^{-1} increase in PI. The LMI of TCs also increases with PI, ranging from 28.5 ms^{-1} to 30.4 ms^{-1} in the warmest and coolest tropopause simulations. This produces a linear regression rate of 0.26 ms^{-1} increase in LMI per 1 ms^{-1} increase in PI. As for TC frequency and TC LMI, we find a significant correlation between global mean annual ACE and the spread in PI as dictated by upper tropospheric temperature differences. Global mean annual ACE increases by ∼29% from the warmest and coolest tropopause simulations. The computed sensitivity is 29 units of ACE per 1 ms^{-1} increase in PI.

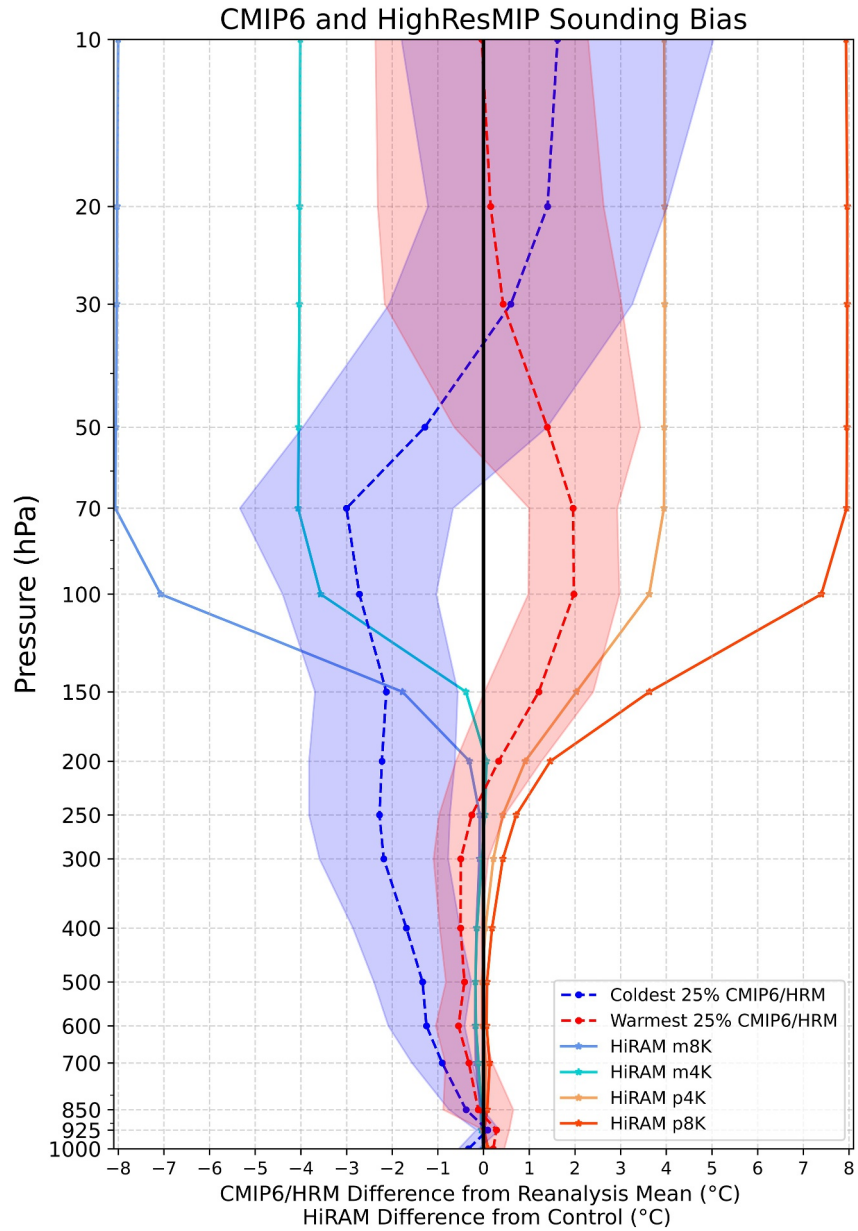

Figure 2. Difference of the coldest 25% and warmest 25% Coupled Model Intercomparison Project 6 and HighResMIP (HRM) temperature profiles from the mean of MERRA2 and ERA5 reanalysis, where coldest and warmest are determined by 70–150 hPa layer mean temperature. HiRAM simulations with modified upper atmospheric temperature profiles are shown as a difference from the HiRAM control simulation.

The response of TC activity to outflow temperatures varies between TC basins. For the basin analyses, we consider the mean PI where PI is greater than or equal to 50 ms^{-1}. Considering PI in excess of a threshold eliminates the need to define basin seasonality, and is similar in approach to the genesis potential index derived in K. Emanuel (2010). Figure S4 in Supporting Information S1 shows average annual TC frequency in each simulation for individual TC basins. The WPAC presents the strongest relationship between the spread in PI driven by outflow temperatures and mean annual TC frequency, ranging from 25 to 39 TCs on average per year within the warmest and coolest tropopause simulations, respectively. The rate of increase of TC frequency in the WPAC of 1.7 TCs per 1 ms^{-1} increase in PI is only approached by that of the SIO, where mean annual TC frequency increases by about 0.7 TCs per 1 ms^{-1}. This suggests that the global relationship between mean annual TC frequency and differences in PI driven by tropopause temperatures is therefore dominated by intra-basin

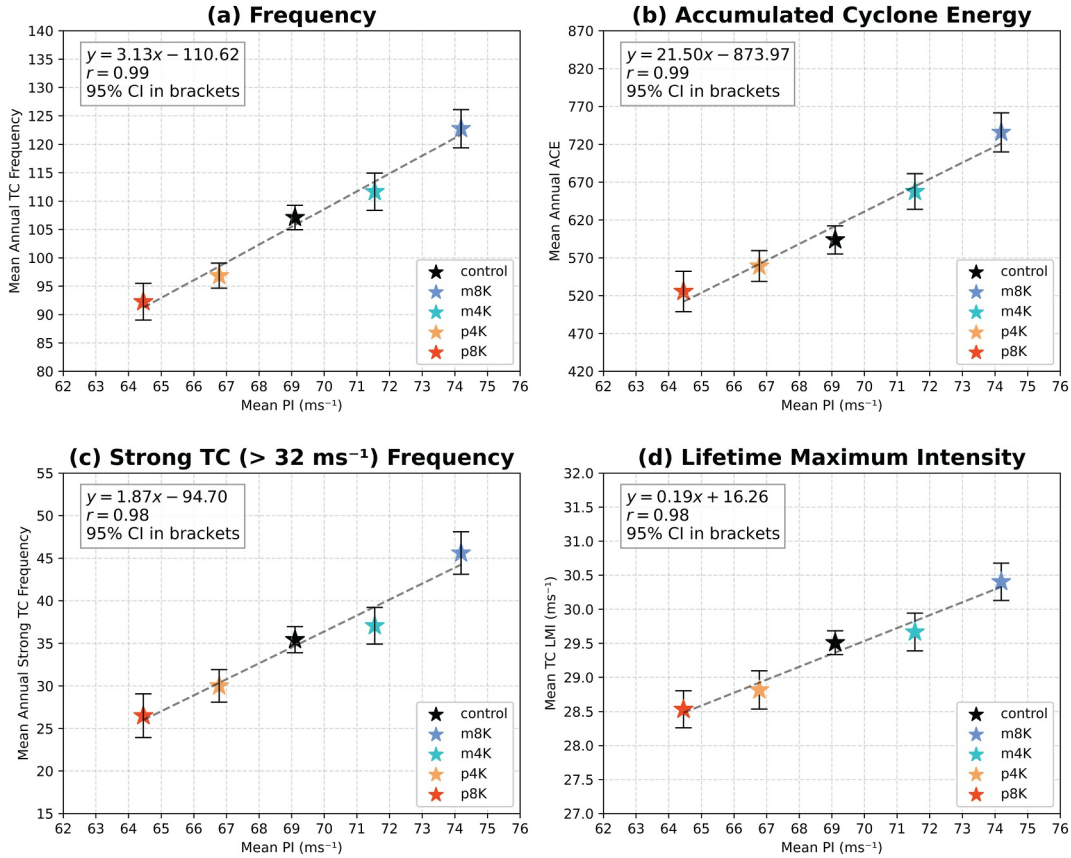

Figure 3. Tropical mean potential intensity (PI) and (a) global mean annual tropical cyclone (TC) frequency, (b) global mean annual accumulated cyclone energy (ACE; unitless), (c) global mean strong TC frequency, and (d) global mean lifetime maximum intensity in the HiRAM m8K (purple), m4K (blue), control (black), p4K (orange), and p8K (red) simulations. 95% confidence intervals are indicated by the brackets.

changes in the WPAC and SIO. The changes in TC frequency within these two basins could suggest greater relevance of tropopause temperature and PI to tropical cyclogenesis than in other TC ocean basins. The Seed Propensity Index (SPI; Hsieh et al., 2022), which assesses climate scale favorability for disturbances that could precede tropical cyclogenesis, increases in the WPAC by 20% relative to the control for the m8K simulation (not shown). The SPI shows no signal in the SIO. The WPAC and SIO also present the largest rates of change of strong TCs per change in PI at 1.0 per 1 ms^{-1} and 0.35 per 1 ms^{-1}, respectively. Notably, the NATL shows an increase in strong TCs of 0.33 per 1 ms^{-1}, approximately doubling the frequency of strong TCs between the warmest and coolest tropopause simulations. Basin scale results for strong TC frequency are shown in Figure S5 in Supporting Information S1.

The response of LMI to different PI and tropopause temperature is positive in all basins except the SATL (Figure S6 in Supporting Information S1). The NATL has the largest sensitivity, followed by the CPAC and WPAC. Compared to TC frequency, TC LMI responds to PI and tropopause temperatures in more ocean basins. The global response, however, is likely dominated by signals in the NATL, CPAC, and WPAC. The global sensitivity of TC ACE is dominated by the WPAC (13.8 units per 1 ms^{-1}). Positive relationships of lesser magnitudes are found in the SIO (3.9 units per 1 ms^{-1}), NATL (2.9 units per 1 ms^{-1}), and NIO (1.2 units per 1 ms^{-1}). Other TC basins are flat or insignificantly correlated (Figure S7 in Supporting Information S1).

Across all TC activity metrics, the WPAC presents the strongest and most significant response to changes in PI driven by differences in outflow temperatures. This response, relative to the other basins, echoes findings from prior work that indicate the WPAC is more sensitive to different outflow temperatures because TC outflow in this basin extends to the lower stratosphere, at higher altitude than other ocean basins (Gilford et al., 2017).

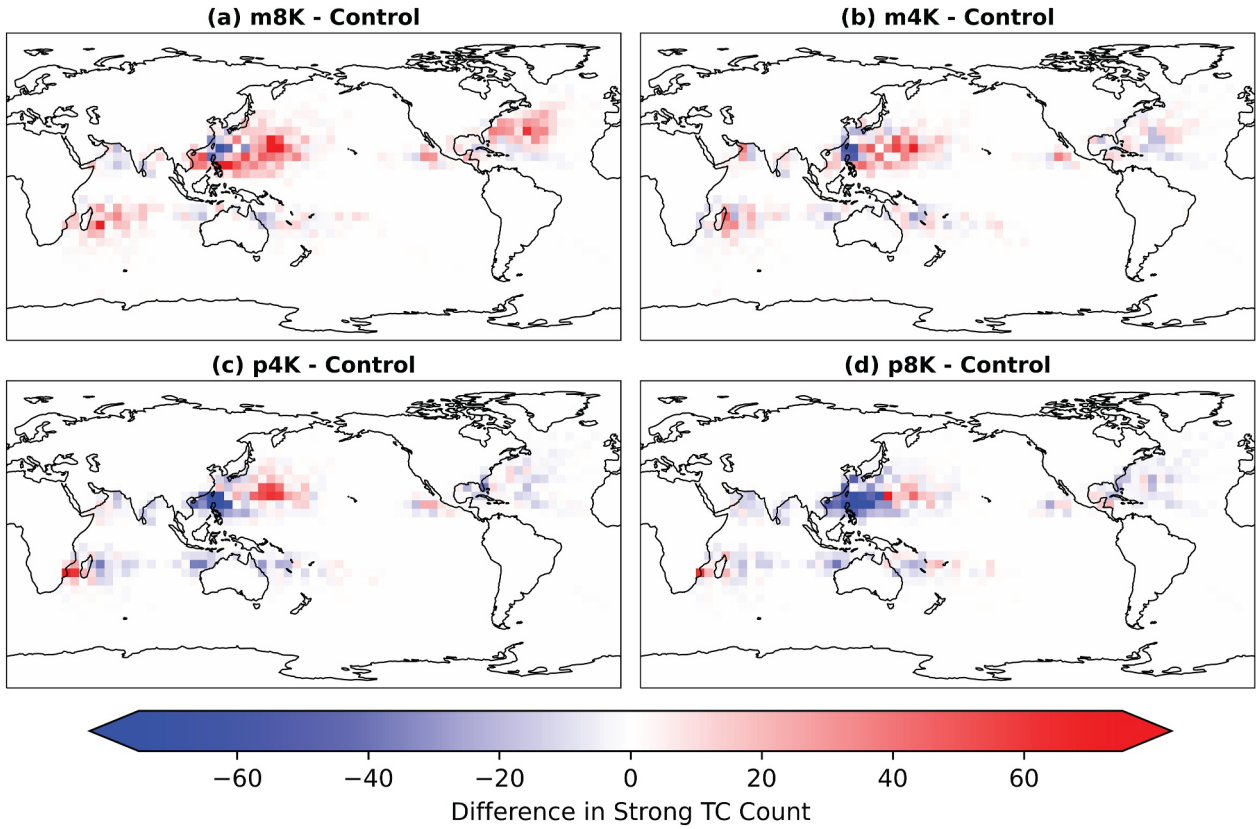

Figure 4. Change in strong TC track density relative to the HiRAM control simulation for (a) m8K, (b) m4K, (c) p4K, and (d) p8K. Track density is the total number of TC tracks in each 5° × 5° latitude/longitude bin.

Additionally, Gilford et al. (2019) and Shields et al. (2020) strongly relate PI to seasonal TC intensity in the WPAC basin.

We also consider spatial changes in PI relative to the HiRAM control, shown in Figure S8 in Supporting Information S1. The largest changes in PI are generally confined within 30°S to 30°N, except in the western Atlantic where highest magnitude changes in PI extend to 45°N. Recognizing that PI is most likely to influence strong TC activity, we first examine changes in strong TC track density (Figure 4). The NATL, WPAC, and SIO, which exhibited the largest changes in mean annual strong TC frequency with PI, all have notable increases in strong TC track density with increasing PI. The NATL has more strong TCs tracking in the subtropics through the western Atlantic. The WPAC has a strong signal near southeastern Asia, but we note an area of positive track densities in all simulations relative to the control in the eastern WPAC. The cause of these positive track densities is unknown yet seemingly unrelated to differences in PI, given the significant basin-wide responses discussed previously. In the SIO, the strongest signal is in the central and western basin near Madagascar. There are also persistently positive TC track densities in the Mozambique Channel. Spatial changes in TC tracks for all TCs is shown in Figure S9 in Supporting Information S1. The results for all TCs are largely consistent with that of strong TCs in the WPAC and SIO, but in other basins the spatial changes are more subtle. In the NATL, there is a near constant spatial difference in TC tracks relative to the control, that is, consistent with the flat response of TC frequency in Figure S4 in Supporting Information S1. In the m8K simulations, NATL TC tracks shift poleward. This could be a consequence of creating a more unstable vertical temperature profile while holding surface boundary conditions constant, in a basin with a large meridional extent and a higher tropopause pressure (lower altitude) than the WPAC. Areas with persistently positive changes in track density identified in Figure 4 are also evident in Figure S9 in Supporting Information S1.

4. Conclusions

In this work, we demonstrated a strong relationship between PI and outflow temperatures across CMIP6 models and HighResMIP models, which complements existing theories of PI sensitivity to a model's mean state including SST (K. Emanuel et al., 2013; Ramsay, 2013; Wing et al., 2015). Specifically, our results highlight that cooler tropopause and stratospheric temperatures provide for cooler outflow temperatures and higher PI.

Using a TC-permitting global climate model, a series of experiments were conducted to elucidate the influence of the tropopause and stratospheric temperature on PI and TC activity. When temperature at and above the local tropopause is nudged to a warmer state, the model-simulated global TC activity decreases, as illustrated by annual mean TC frequency, annual mean ACE, and annual mean LMI. However, the responses of TC activity to tropopause and stratospheric temperature perturbations vary between ocean basins, and it appears that some individual basins dominate the apparent global signal. The spatial response of TCs and strong TCs to the different temperature regimes is maximized in the midlatitudes, especially for changes in strong TC tracks in the NATL. This pattern resembles the poleward migration of TC LMI locations, which prior studies have shown to correspond to more supportive PI at higher latitudes (Daloz & Camargo, 2018; Kossin et al., 2014; Studholme et al., 2022). We increased the PI in all ocean basins without changing the SST, increasing the thermodynamic favorability for TCs in the subtropics that could allow for poleward migration between model simulations.

The demonstrated dependence of TC activity on stratosphere temperature within the HiRAM simulations suggests the inter-model spread in the upper tropospheric temperature profile found in the HighResMIP historical simulations likely impact the intrinsically resolved TCs. Future work, including future versions of the HighResMIP protocol, should consider this relationship when assessing changes in the TC climatology in historical and future climates.

Conflict of Interest

The authors declare no conflicts of interest relevant to this study.

Data Availability Statement

HiRAM simulations were performed on Princeton University Research Computing systems. Post-processed data from the HiRAM simulations necessary for reproduction of these results is available in Mahoney (2024a, 2024b). ERA5 data (Hersbach et al., 2020) was obtained via the Copernicus Climate Data Store at Hersbach et al. (2023a, 2023b). MERRA2 data was obtained at Global Modeling And Assimilation Office, & Pawson, S. (2015a, 2015b). CMIP6 (Eyring et al., 2016) and HighResMIP (Haarsma et al., 2016) data sets are both archived in a repository hosted by the Lawrence Livermore National Laboratory and Earth System Grid Federation at https://aims2.llnl.gov/search/cmip6/.

Acknowledgments
The authors thank Kerry Emanuel and an anonymous reviewer for comments which significantly improved the quality of this manuscript. This research was supported by National Aeronautics and Space Administration Award 80NSSC25K7181 and National Oceanic and Atmospheric Administration Award NA21OAR4310351. This work is also supported in part by the Simons Foundation. We are grateful to Princeton University Research Computing, where HiRAM simulations were run. Aidan D. Mahoney is also a Pathways Intern at the National Oceanic and Atmospheric Administration (NOAA) National Weather Service National Hurricane Center. The research documented here was conducted solely under his capacity at and affiliation with the University of Miami.

References

Alland, J. J., Tang, B. H., Corbosiero, K. L., & Bryan, G. H. (2021a). Combined effects of midlevel dry air and vertical wind shear on tropical cyclone development. Part I: Downdraft ventilation. *Journal of the Atmospheric Sciences*, *78*(3), 763–782. https://doi.org/10.1175/JAS-D-20-0054.1

Alland, J. J., Tang, B. H., Corbosiero, K. L., & Bryan, G. H. (2021b). Combined effects of midlevel dry air and vertical wind shear on tropical cyclone development. Part II: Radial ventilation. *Journal of the Atmospheric Sciences*, *78*(3), 783–796. https://doi.org/10.1175/JAS-D-20-0055.1

Bell, G. D., Halpert, M. S., Schnell, R. C., Higgins, R. W., Lawrimore, J., Kousky, V. E., et al. (2000). Climate assessment for 1999. *Bulletin of the American Meteorological Society*, *81*(6), s1–s50. https://doi.org/10.1175/1520-0477(2000)81%255Bs1:CAF%255D2.0.CO;2

Bhatia, K., Baker, A., Yang, W., Vecchi, G., Knutson, T., Murakami, H., et al. (2022). A potential explanation for the global increase in tropical cyclone rapid intensification. *Nature Communications*, *13*(1), 6626. https://doi.org/10.1038/s41467-022-34321-6

Bister, M., & Emanuel, K. A. (1998). Dissipative heating and hurricane intensity. *Meteorology and Atmospheric Physics*, *65*(3–4), 233–240. https://doi.org/10.1007/BF01030791

Bister, M., & Emanuel, K. A. (2002). Low frequency variability of tropical cyclone potential intensity 1. Interannual to interdecadal variability. *Journal of Geophysical Research*, *107*(D24). https://doi.org/10.1029/2001JD000776

Broccoli, A. J., & Manabe, S. (1990). Can existing climate models be used to study anthropogenic changes in tropical cyclone climate? *Geophysical Research Letters*, *17*(11), 1917–1920. https://doi.org/10.1029/GL017i011p01917

Bruyère, C. L., Holland, G. J., & Towler, E. (2012). Investigating the use of a genesis potential index for tropical cyclones in the North Atlantic Basin. *Journal of Climate*, *25*(24), 8611–8626. https://doi.org/10.1175/JCLI-D-11-00619.1

Camargo, S. J., Emanuel, K. A., & Sobel, A. H. (2007). Use of a genesis potential index to diagnose ENSO effects on tropical cyclone genesis. *Journal of Climate*, *20*(19), 4819–4834. https://doi.org/10.1175/JCLI4282.1

Camargo, S. J., Giulivi, C. F., Sobel, A. H., Wing, A. A., Kim, D., Moon, Y., et al. (2020). Characteristics of model tropical cyclone climatology and the large-scale environment. *Journal of Climate*, *33*(11), 4463–4487. https://doi.org/10.1175/JCLI-D-19-0500.1

Camargo, S. J., Sobel, A. H., Barnston, A. G., & Emanuel, K. A. (2007). Tropical cyclone genesis potential index in climate models. *Tellus A: Dynamic Meteorology and Oceanography*, *59*(4), 428. https://doi.org/10.1111/j.1600-0870.2007.00238.x

Camargo, S. J., Tippett, M. K., Sobel, A. H., Lee, C.-Y., Fosu, B., & Hodges, K. I. (2025). Tropical cyclones and associated environmental fields in CMIP6 models. *Journal of Climate*, *38*(15), 3877–3902. https://doi.org/10.1175/JCLI-D-24-0629.1

Camargo, S. J., Tippett, M. K., Sobel, A. H., Vecchi, G. A., & Zhao, M. (2014). Testing the performance of tropical cyclone genesis indices in future climates using the HiRAM model. *Journal of Climate*, *27*(24), 9171–9196. https://doi.org/10.1175/JCLI-D-13-00505.1

Camargo, S. J., & Wing, A. A. (2016). Tropical cyclones in climate models. *WIREs Climate Change*, *7*(2), 211–237. https://doi.org/10.1002/wcc.373

Chavas, D. R., Camargo, S. J., & Tippett, M. K. (2024). Tropical cyclone genesis potential using a ventilated potential intensity. *Journal of Climate*, *38*(7), 1667–1689. https://doi.org/10.1175/JCLI-D-24-0186.1

Craig, G. C., & Gray, S. L. (1996). CISK or WISHE as the mechanism for tropical cyclone intensification. *Journal of the Atmospheric Sciences*, *53*(23), 3528–3540. https://doi.org/10.1175/1520-0469(1996)053<3528:COWATM>2.0.CO;2

Daloz, A. S., & Camargo, S. J. (2018). Is the poleward migration of tropical cyclone maximum intensity associated with a poleward migration of tropical cyclone genesis? *Climate Dynamics*, *50*(1–2), 705–715. https://doi.org/10.1007/s00382-017-3636-7

Dirkes, C. A., Wing, A. A., Camargo, S. J., & Kim, D. (2023). Process-Oriented diagnosis of tropical cyclones in reanalyses using a moist static energy variance budget. *Journal of Climate*, *36*(16), 5293–5317. https://doi.org/10.1175/JCLI-D-22-0384.1

Elsner, J. B., Kossin, J. P., & Jagger, T. H. (2008). The increasing intensity of the strongest tropical cyclones. *Nature*, *455*(7209), 92–95. https://doi.org/10.1038/nature07234

Emanuel, K. (2010). Tropical cyclone activity downscaled from NOAA-CIRES Reanalysis, 1908–1958. *Journal of Advances in Modeling Earth Systems*, *2*(1). JAMES.2010.2.1. https://doi.org/10.3894/JAMES.2010.2.1

Emanuel, K., Solomon, S., Folini, D., Davis, S., & Cagnazzo, C. (2013). Influence of tropical tropopause layer cooling on Atlantic hurricane activity. *Journal of Climate*, *26*(7), 2288–2301. https://doi.org/10.1175/JCLI-D-12-00242.1

Emanuel, K. A. (1986). An air-sea interaction theory for tropical cyclones. Part I: Steady-state maintenance. *Journal of the Atmospheric Sciences*, *43*(6), 585–605. https://doi.org/10.1175/1520-0469(1986)043<0585:aasitf>2.0.co;2

Emanuel, K. A., David Neelin, J., & Bretherton, C. S. (1994). On large-scale circulations in convecting atmospheres. *Quarterly Journal of the Royal Meteorological Society*, *120*(519), 1111–1143. https://doi.org/10.1002/qj.49712051902

Emanuel, K. A., & Nolan, D. S. (2004). Tropical cyclone activity and global climate (pp. 240–241).

Eyring, V., Bony, S., Meehl, G. A., Senior, C. A., Stevens, B., Stouffer, R. J., & Taylor, K. E. (2016). Overview of the Coupled Model Intercomparison Project Phase 6 (CMIP6) experimental design and organization. *Geoscientific Model Development*, *9*(5), 1937–1958. https://doi.org/10.5194/gmd-9-1937-2016

Finocchio, P. M., Majumdar, S. J., Nolan, D. S., & Iskandarani, M. (2016). Idealized tropical cyclone responses to the height and depth of environmental vertical wind shear. *Monthly Weather Review*, *144*(6), 2155–2175. https://doi.org/10.1175/MWR-D-15-0320.1

Finocchio, P. M., & Rios-Berrios, R. (2021). The Intensity- and size-dependent response of tropical cyclones to increasing vertical wind shear. *Journal of the Atmospheric Sciences*. https://doi.org/10.1175/JAS-D-21-0126.1

Gilford, D. (2020). dgilford/pyPI: PyPI v1.3 (initial package release) (version v1.3) [Computer software]. *Zenodo*. https://doi.org/10.5281/ZENODO.3985975

Gilford, D. M. (2021). pyPI (v1.3): Tropical cyclone potential intensity calculations in python. *Geoscientific Model Development*, *14*(5), 2351–2369. https://doi.org/10.5194/gmd-14-2351-2021

Gilford, D. M., Solomon, S., & Emanuel, K. A. (2017). On the seasonal cycles of tropical cyclone potential intensity. *Journal of Climate*, *30*(16), 6085–6096. https://doi.org/10.1175/JCLI-D-16-0827.1

Gilford, D. M., Solomon, S., & Emanuel, K. A. (2019). Seasonal cycles of along-track tropical cyclone maximum intensity. *Monthly Weather Review*, *147*(7), 2417–2432. https://doi.org/10.1175/MWR-D-19-0021.1

Global Modeling And Assimilation Office Pawson, S. (2015a). MERRA-2 instM_2d_asm_Nx: 2d,Monthly mean,single-level,assimilation,single-level Diagnostics V5.12.4 [Dataset]. *NASA Goddard Earth Sciences Data and Information Services Center*. https://doi.org/10.5067/5ESKGQTZG7FO

Global Modeling And Assimilation Office Pawson, S. (2015b). MERRA-2 instM_3d_ana_Np: 3d,Monthly mean,Instantaneous,Pressure-Level, Analysis,Analyzed meteorological fields V5.12.4 [Dataset]. *NASA Goddard Earth Sciences Data and Information Services Center*. https://doi.org/10.5067/V92O8XZ30XBI

Gregor, L., & Müller, J. (2022). RECCAP2-ocean shared resources [Dataset]. https://github.com/RECCAP2-ocean/R2-shared-resources

Haarsma, R. J., Roberts, M. J., Vidale, P. L., Senior, C. A., Bellucci, A., Bao, Q., et al. (2016). High resolution model Intercomparison Project (HighResMIP v1.0) for CMIP6. *Geoscientific Model Development*, *9*(11), 4185–4208. https://doi.org/10.5194/gmd-9-4185-2016

Harris, L. M., Lin, S.-J., & Tu, C. (2016). High-Resolution climate simulations using GFDL HiRAM with a stretched global grid. *Journal of Climate*, *29*(11), 4293–4314. https://doi.org/10.1175/JCLI-D-15-0389.1

Hersbach, H., Bell, B., Berrisford, P., Biavati, G., Horányi, A., Muñoz Sabater, J., et al. (2023a). ERA5 monthly averaged data on pressure levels from 1940 to present [Dataset]. *Copernicus Climate Change Service (C3S) Climate Data Store (CDS)*. https://doi.org/10.24381/cds.6860a573

Hersbach, H., Bell, B., Berrisford, P., Biavati, G., Horányi, A., Muñoz Sabater, J., et al. (2023b). ERA5 monthly averaged data on single levels from 1940 to present [Dataset]. *Copernicus Climate Change Service (C3S) Climate Data Store (CDS)*. https://doi.org/10.24381/cds.f17050d7

Hersbach, H., Bell, B., Berrisford, P., Hirahara, S., Horányi, A., Muñoz-Sabater, J., et al. (2020). The ERA5 global reanalysis. *Quarterly Journal of the Royal Meteorological Society*, *146*(730), 1999–2049. https://doi.org/10.1002/qj.3803

Hodges, K., Cobb, A., & Vidale, P. L. (2017). How well are tropical cyclones represented in reanalysis datasets? *Journal of Climate*, *30*(14), 5243–5264. https://doi.org/10.1175/JCLI-D-16-0557.1

Hsieh, T., Yang, W., Vecchi, G. A., & Zhao, M. (2022). Model spread in the tropical cyclone frequency and seed propensity index across global warming and ENSO-Like perturbations. *Geophysical Research Letters*, *49*(7), e2021GL097157. https://doi.org/10.1029/2021GL097157

Kennedy, J., Titchner, H., Rayner, N., & Roberts, M. (2017). input4MIPs.MOHC.SSTsAndSeaIce.HighResMIP.MOHC-HadISST-2-2-0-0-0 (version 20230220) [Application/x-netcdf]. *Earth System Grid Federation*. https://doi.org/10.22033/ESGF/INPUT4MIPS.1221

Kim, D., Moon, Y., Camargo, S. J., Wing, A. A., Sobel, A. H., Murakami, H., et al. (2018). Process-Oriented diagnosis of tropical cyclones in high-resolution GCMs. *Journal of Climate*, *31*(5), 1685–1702. https://doi.org/10.1175/JCLI-D-17-0269.1

Klotzbach, P. J., Bowen, S. G., Pielke, R., & Bell, M. (2018). Continental U.S. hurricane landfall frequency and associated damage: Observations and future risks. *Bulletin of the American Meteorological Society*, *99*(7), 1359–1376. https://doi.org/10.1175/BAMS-D-17-0184.1

Knutson, T., Camargo, S. J., Chan, J. C. L., Emanuel, K., Ho, C.-H., Kossin, J., et al. (2020). Tropical cyclones and climate change assessment: Part II: Projected response to anthropogenic warming. *Bulletin of the American Meteorological Society*, *101*(3), E303–E322. https://doi.org/10.1175/BAMS-D-18-0194.1

Kossin, J. P. (2015). Validating atmospheric reanalysis data using tropical cyclones as thermometers. *Bulletin of the American Meteorological Society*, *96*(7), 1089–1096. https://doi.org/10.1175/BAMS-D-14-00180.1

Kossin, J. P., Emanuel, K. A., & Vecchi, G. A. (2014). The poleward migration of the location of tropical cyclone maximum intensity. *Nature*, *509*(7500), 349–352. https://doi.org/10.1038/nature13278

Kossin, J. P., Knapp, K. R., Olander, T. L., & Velden, C. S. (2020). Global increase in major tropical cyclone exceedance probability over the past four decades. *Proceedings of the National Academy of Sciences*, *117*(22), 11975–11980. https://doi.org/10.1073/pnas.1920849117

Kossin, J. P., Olander, T. L., & Knapp, K. R. (2013). Trend analysis with a new global record of tropical cyclone intensity. *Journal of Climate*, *26*(24), 9960–9976. https://doi.org/10.1175/JCLI-D-13-00262.1

Kreussler, P., Caron, L., Wild, S., Loosveldt Tomas, S., Chauvin, F., Moine, M., et al. (2021). Tropical cyclone integrated kinetic energy in an ensemble of HighResMIP simulations. *Geophysical Research Letters*, *48*(5), e2020GL090963. https://doi.org/10.1029/2020GL090963

Mahoney, A. (2024a). HiRAM Control Simulation Data for "The Influence of Tropopause Temperature Biases on Climate Model Simulations of Tropical Cyclones" (Version v1) [Dataset]. *Zenodo*. https://doi.org/10.5281/ZENODO.14416185

Mahoney, A. (2024b). HiRAM simulations with nudged upper tropospheric temperatures data for "The Influence of Tropopause Temperature Biases on Climate Model Simulations of Tropical Cyclones" (Version v1) [Dataset]. *Zenodo*. https://doi.org/10.5281/ZENODO.14416702

Mischell, E., Soden, B., Zhang, B., Hsieh, T., & Vecchi, G. (2024). Why does atmospheric radiative heating weaken midlatitude cyclones? *Geophysical Research Letters*, *51*(19), e2024GL110754. https://doi.org/10.1029/2024GL110754

Moon, Y., Kim, D., Camargo, S. J., Wing, A. A., Sobel, A. H., Murakami, H., et al. (2020). Azimuthally averaged wind and thermodynamic structures of tropical cyclones in global climate models and their sensitivity to horizontal resolution. *Journal of Climate*, *33*(4), 1575–1595. https://doi.org/10.1175/JCLI-D-19-0172.1

Moon, Y., Kim, D., Wing, A. A., Camargo, S. J., Zhao, M., Leung, L. R., et al. (2022). An evaluation of tropical cyclone rainfall structures in the HighResMIP simulations against satellite observations. *Journal of Climate*, *35*(22), 7315–7338. https://doi.org/10.1175/JCLI-D-21-0564.1

Ramsay, H. A. (2013). The effects of imposed stratospheric cooling on the maximum intensity of tropical cyclones in axisymmetric radiative–convective equilibrium. *Journal of Climate*, *26*(24), 9977–9985. https://doi.org/10.1175/JCLI-D-13-00195.1

Rappaport, E. N. (2014). Fatalities in the United States from Atlantic tropical cyclones: New data and interpretation. *Bulletin of the American Meteorological Society*, *95*(3), 341–346. https://doi.org/10.1175/BAMS-D-12-00074.1

Rayner, N. A., Parker, D. E., Horton, E. B., Folland, C. K., Alexander, L. V., Rowell, D. P., et al. (2003). Global analyses of sea surface temperature, sea ice, and night marine air temperature since the late nineteenth century. *Journal of Geophysical Research*, *108*(D14), 2002JD002670. https://doi.org/10.1029/2002JD002670

Rios-Berrios, R., Finocchio, P. M., Alland, J. J., Chen, X., Fischer, M. S., Stevenson, S. N., & Tao, D. (2024). A review of the interactions between tropical cyclones and environmental vertical wind shear. *Journal of the Atmospheric Sciences*, *81*(4), 713–741. https://doi.org/10.1175/JAS-D-23-0022.1

Roberts, M. J., Camp, J., Seddon, J., Vidale, P. L., Hodges, K., Vanniere, B., et al. (2020a). Impact of model resolution on tropical cyclone simulation using the HighResMIP–PRIMAVERA multimodel ensemble. *Journal of Climate*, *33*(7), 2557–2583. https://doi.org/10.1175/JCLI-D-19-0639.1

Roberts, M. J., Camp, J., Seddon, J., Vidale, P. L., Hodges, K., Vannière, B., et al. (2020b). Projected future changes in tropical cyclones using the CMIP6 HighResMIP Multimodel ensemble. *Geophysical Research Letters*, *47*(14), e2020GL088662. https://doi.org/10.1029/2020GL088662

Shields, S., Wing, A. A., & Gilford, D. M. (2020). A global analysis of interannual variability in potential and actual tropical cyclone intensities. *Geophysical Research Letters*, *47*(18), e2020GL089512. https://doi.org/10.1029/2020GL089512

Sobel, A. H., Camargo, S. J., Hall, T. M., Lee, C.-Y., Tippett, M. K., & Wing, A. A. (2016). Human influence on tropical cyclone intensity. *Science*, *353*(6296), 242–246. https://doi.org/10.1126/science.aaf6574

Starr, J. C., Wing, A. A., Camargo, S. J., Kim, D., Lee, T.-Y., & Moon, J. (2025). Using the moist static energy variance budget to evaluate tropical cyclones in climate models against reanalyses and satellite observations. *Journal of Climate*, *38*(14), 3353–3379. https://doi.org/10.1175/JCLI-D-24-0353.1

Studholme, J., Fedorov, A. V., Gulev, S. K., Emanuel, K., & Hodges, K. (2022). Poleward expansion of tropical cyclone latitudes in warming climates. *Nature Geoscience*, *15*(1), 14–28. https://doi.org/10.1038/s41561-021-00859-1

Tang, B., & Emanuel, K. (2010). Midlevel ventilation's constraint on tropical cyclone intensity. *Journal of the Atmospheric Sciences*, *67*(6), 1817–1830. https://doi.org/10.1175/2010JAS3318.1

Tang, B., & Emanuel, K. (2012). Sensitivity of tropical cyclone intensity to ventilation in an axisymmetric model. *Journal of the Atmospheric Sciences*, *69*(8), 2394–2413. https://doi.org/10.1175/JAS-D-11-0232.1

Trabing, B. C., Bell, M. M., & Brown, B. R. (2019). Impacts of radiation and upper-tropospheric temperatures on tropical cyclone structure and intensity. *Journal of the Atmospheric Sciences*, *76*(1), 135–153. https://doi.org/10.1175/JAS-D-18-0165.1

Ullrich, P. A., & Zarzycki, C. M. (2017). TempestExtremes: A framework for scale-insensitive pointwise feature tracking on unstructured grids. *Geoscientific Model Development*, *10*(3), 1069–1090. https://doi.org/10.5194/gmd-10-1069-2017

Vecchi, G. A., Fueglistaler, S., Held, I. M., Knutson, T. R., & Zhao, M. (2013). Impacts of atmospheric temperature trends on tropical cyclone activity. *Journal of Climate*, *26*(11), 3877–3891. https://doi.org/10.1175/JCLI-D-12-00503.1

Walsh, K. J. E., McBride, J. L., Klotzbach, P. J., Balachandran, S., Camargo, S. J., Holland, G., et al. (2016). Tropical cyclones and climate change. *WIREs Climate Change*, *7*(1), 65–89. https://doi.org/10.1002/wcc.371

Wang, B., & Murakami, H. (2020). Dynamic genesis potential index for diagnosing present-day and future global tropical cyclone genesis. *Environmental Research Letters*, *15*(11), 114008. https://doi.org/10.1088/1748-9326/abbb01

Wing, A. A., Camargo, S. J., Sobel, A. H., Kim, D., Moon, Y., Murakami, H., et al. (2019). Moist static energy budget analysis of tropical cyclone intensification in high-resolution climate models. *Journal of Climate*, *32*(18), 6071–6095. https://doi.org/10.1175/JCLI-D-18-0599.1

Wing, A. A., Emanuel, K., & Solomon, S. (2015). On the factors affecting trends and variability in tropical cyclone potential intensity: Potential INTENSITY TRENDS AND VARIABILITY. *Geophysical Research Letters*, *42*(20), 8669–8677. https://doi.org/10.1002/2015GL066145

World Meteorological Organization. (1957). Definition of the tropopause. *WMO Bull*, *6*, 136.

Zarzycki, C. M., & Ullrich, P. A. (2017). Assessing sensitivities in algorithmic detection of tropical cyclones in climate data. *Geophysical Research Letters*, *44*(2), 1141–1149. https://doi.org/10.1002/2016GL071606

Zhao, M., & Held, I. M. (2010). An analysis of the effect of global warming on the intensity of Atlantic hurricanes using a GCM with statistical refinement. *Journal of Climate*, *23*(23), 6382–6393. https://doi.org/10.1175/2010JCLI3837.1

Zhao, M., & Held, I. M. (2012). TC-Permitting GCM simulations of hurricane frequency response to Sea surface temperature anomalies projected for the late-twenty-first century. *Journal of Climate*, *25*(8), 2995–3009. https://doi.org/10.1175/JCLI-D-11-00313.1

Zhao, M., Held, I. M., Lin, S.-J., & Vecchi, G. A. (2009). Simulations of global hurricane climatology, interannual variability, and response to global warming using a 50-km resolution GCM. *Journal of Climate*, *22*(24), 6653–6678. https://doi.org/10.1175/2009JCLI3049.1

Zhao, M., Held, I. M., & Vecchi, G. A. (2010). Retrospective forecasts of the hurricane season using a global atmospheric model assuming persistence of SST anomalies. *Monthly Weather Review*, *138*(10), 3858–3868. https://doi.org/10.1175/2010MWR3366.1